

# Final Project Report: Angle Optimization of the AstroJays Rocket Nozzle

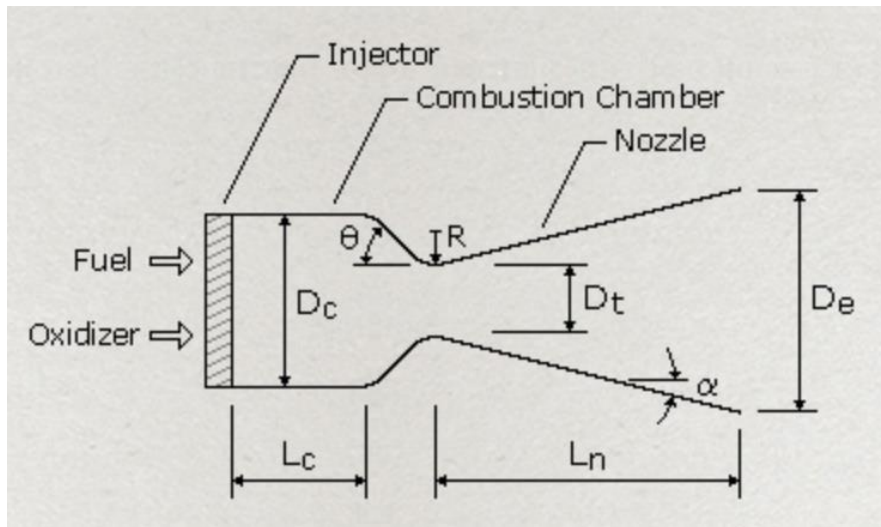
Alex Ren

EN.530.483/683 Applied Computational Modeling

## Introduction and Background

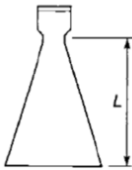
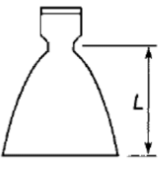
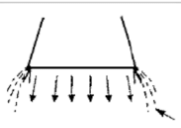
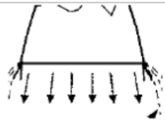
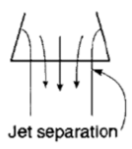
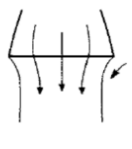
Nozzles are mechanical devices which are used to control the flow characteristics of a fluid as the fluid enters or exits an enclosed chamber or pipe [1]. Nozzles can typically be categorized into two types: a converging nozzle and a diverging nozzle. In a converging nozzle, the diameter of the nozzle decreases in the direction of the fluid flow whereas in a diverging nozzle, the diameter of the nozzle increases in the direction of the fluid flow. Nozzles control the pressure, direction, and flow rate of the fluid passing through them.

One of the most common types of nozzles used in rocket engines is the convergent-divergent (CD) nozzle, also known as the de-Laval nozzle [2]. There are three sections in a CD nozzle. These sections are the converging section, the throat, and the diverging section (Fig.1).



**Figure 1.** Diagram of converging-divergent nozzle [3]. Angle  $\theta$  is the convergence half-angle and angle  $\alpha$  is the divergence half-angle.

Common configurations of the CD nozzle are the bell-shaped nozzle and the conical nozzle (Fig.2). While the shape of the bell nozzle is more optimized in terms of performance, the conical nozzle is a much simpler geometry to manufacture [4].

	Cone	Bell shaped
Shape		
Flow at high altitude (Under expansion)		
Flow at low altitude (Over-expansion)		

**Figure 2.** Comparison of conical and bell-shaped nozzles [5].

CD nozzles take advantage of the differences in flow characteristics in the subsonic, sonic, and supersonic flow regimes [1]. A properly designed CD nozzle has subsonic flow in the converging section, sonic flow in the throat, and supersonic flow in the diverging section (Fig.3). The converging section compresses the fluid to a higher pressure and accelerates the low velocity fluid to Mach 1 at the throat. The flow becomes sonic at the throat. This phenomenon is called “Choked Flow”, where mass flow rate is at a maximum [6]. In order to further accelerate the fluid flow, a diverging section follows the throat. This allows the fluid to expand and reach supersonic velocity.

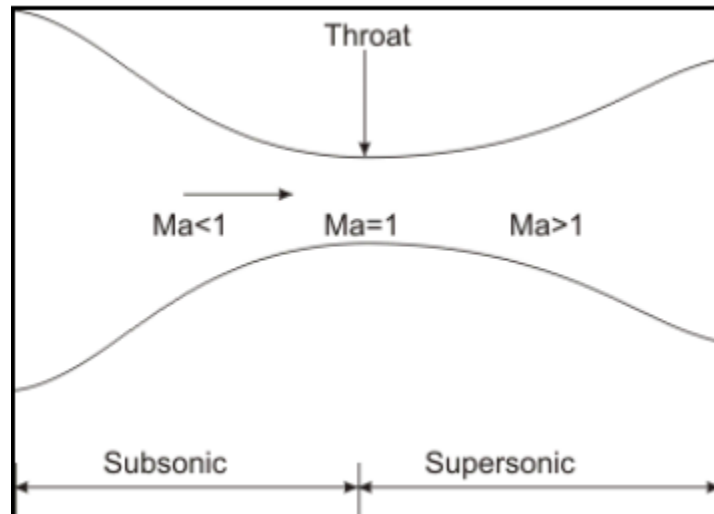


**Figure 3.** Diagram of CD nozzle [1].

The nozzle is a critical component of a rocket engine. The design of the nozzle can significantly affect the thrust produced by the engine. The goal of the nozzle is to maximize the thrust produced by the engine. Equations to calculate the optimal expansion ratio (Eq. 1) and the nozzle

throat area (Eq. 2) provide initial guidance to the design of the nozzle, but are dependent on the assumption that the flow through the nozzle is of a steady, one-dimensional compressible ideal gas [7]. This means that the converging and diverging angles of the nozzle are not considered in these equations.

$$\frac{A_e}{A^*} = \left( \left( \frac{k+1}{2} \right)^{\frac{1}{k-1}} \left( \frac{P_e}{P_0} \right)^{\frac{1}{k}} \sqrt{\frac{k+1}{k-1} \left[ 1 - \left( \frac{P_e}{P_0} \right)^{\frac{k-1}{k}} \right]} \right)^{-1} \quad \text{Eq. 1}$$

$$A^* = F \left( P_0 \sqrt{\frac{2k^2}{k-1} \left( \frac{2}{k+1} \right)^{\frac{(k+1)}{k-1}} \left[ 1 - \left( \frac{P_e}{P_0} \right)^{\frac{k-1}{k}} \right]} \right)^{-1} \quad \text{Eq. 2}$$

In the above equations,  $A_e$  is the exit area,  $A^*$  is the throat area,  $k$  is the ratio of specific heats of the fluid,  $P_e$  is the exit pressure,  $P_0$  is the chamber or inlet pressure, and  $F$  is the thrust produced by the nozzle.

Equations 1 and 2 are also dependent on the properties of the propellant. The propellant that will be used in this analysis is an ammonium perchlorate composite propellant (APCP). The specific propellant mixture is called “Cherry Limeade” and was developed by MIT’s rocketry team.

## Objectives

The objective of this analysis is to optimize the design of the nozzle for the AstroJays solid propellant rocket motor using CFD software. An optimized design is determined by the thrust output of the nozzle which is to be maximized. The inlet, outlet, and throat diameters of the nozzle are to be provided, but the convergence and divergence half-angles remain to be determined. An optimized angle for the converging section will be determined before analyzing the optimized angle for the diverging section. The output thrust will also be calculated for the optimized nozzle design.

## Method

The simulation software that will be used for this analysis is Ansys Fluent and will be conducted using a 3D model.

### *Assumptions*

Several assumptions are made to conduct the simulation. First, the converging and diverging sections of the model will be conical. This is due to the simplicity of manufacturing such a nozzle shape as well as removes the complications of changing angles in a bell-shaped nozzle. Second, the flow is assumed to be inviscid. This assumption is valid due to the high velocities and therefore Reynolds numbers that are expected in the simulation. Third, the propellant is assumed to behave as a compressible ideal gas. Fourth, the combustion process was neglected and replaced with constant inlet boundary conditions. Implementing combustion is beyond the scope of the course and is too complex for the purpose of this project. Last, the walls of the

nozzle are assumed to be adiabatic. The heat transfer through the nozzle walls is negligible compared to the heat transfer by the flow of the propellant.

### Geometry

To form the geometry, a 2D sketch of half the nozzle was created (Fig.4). This consisted of an inlet section, a converging section, and a diverging section. The inlet radius, inlet section length, throat radius, and outlet radius were dimensioned according to the specifications provided (Table 1). Sharp corners in throughout the nozzle were modified to be 0.1" radius fillets. The convergence half-angle and divergence half-angle were also modified according to the different values to be simulated. Convergence half-angles will be analyzed in the range of 10-80° while the divergence half-angles will be analyzed in the range of 10-18°.

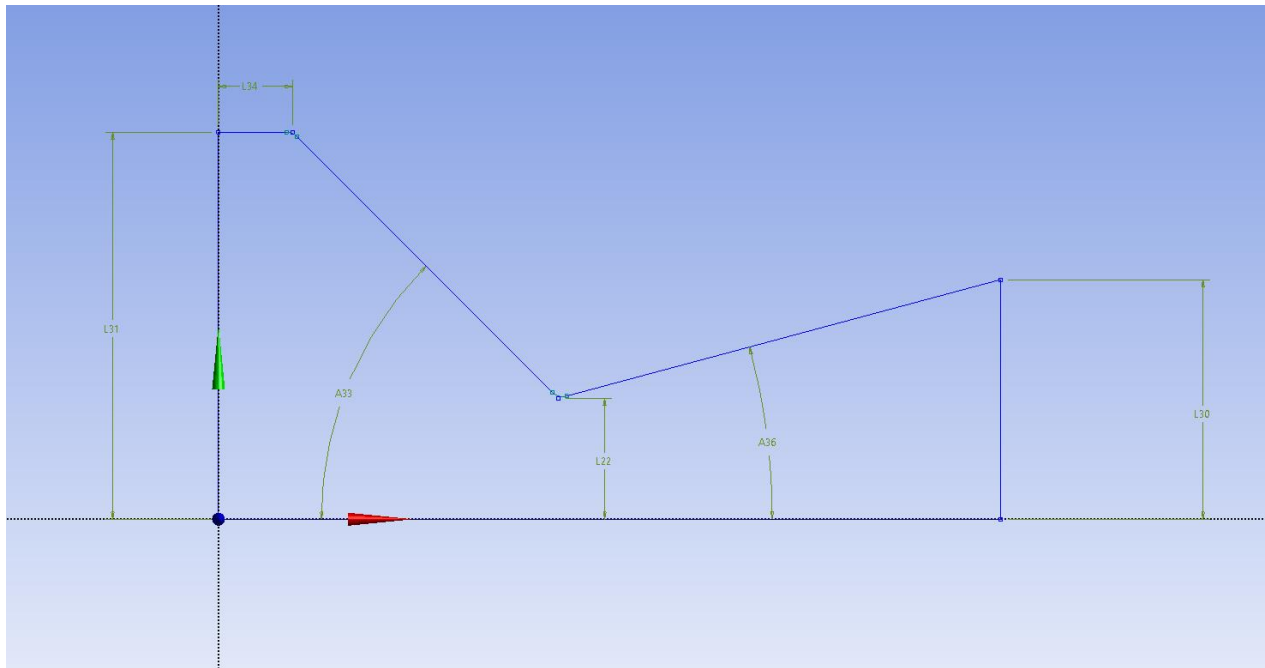


**Figure 4.** 2D sketch of half nozzle. L31 is the inlet radius, L34 is the length of the inlet section, L22 is the throat radius, L30 is the exit radius, A33 is the convergence half-angle, and A36 is the divergence half-angle.

**Table 1.** Parameters for nozzle geometry

Parameter	Value
Inlet Diameter	2.65 in
Throat Diameter	0.82 in
Exit Diameter	1.68 in
Inlet Section Length	0.25 in

The 2D sketch was revolved around the center axis to form a 3D model of the nozzle (Fig.5). This 3D nozzle is the geometry to be analyzed with Ansys Fluent.

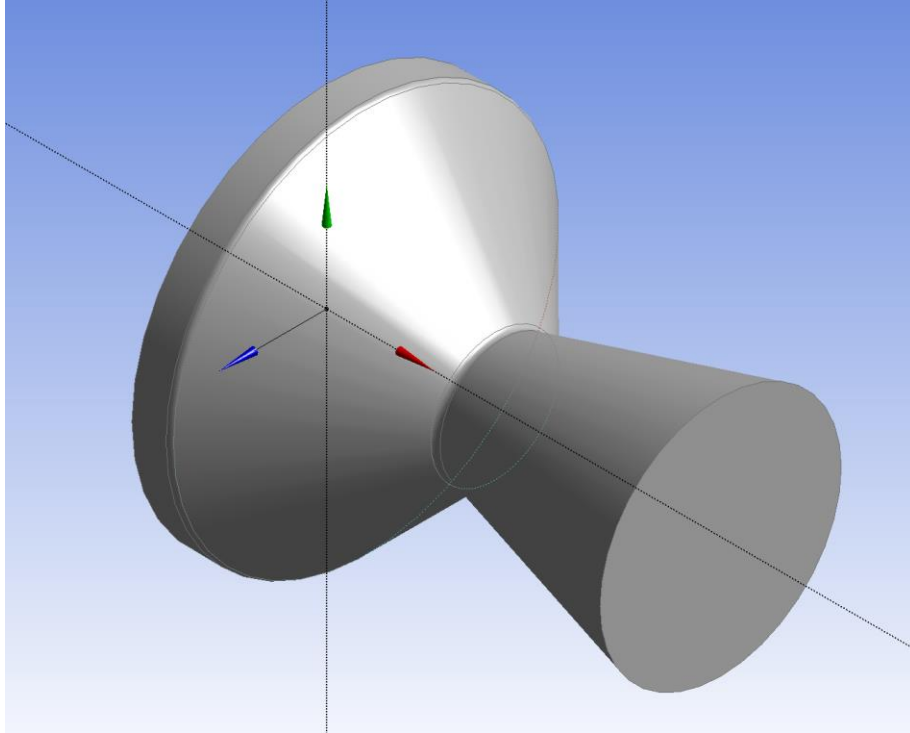


**Figure 5.** 3D nozzle geometry. The 3D geometry was created by revolving the 2D sketch around the x-axis.

### *Meshing*

The inlet, outlet, and walls of the nozzle were defined as named selections (Fig.6).

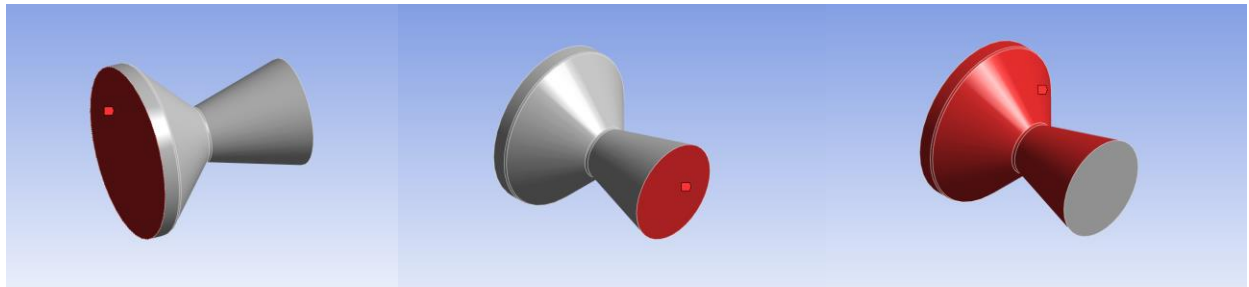


**Figure 6.** From left to right: inlet, outlet, and wall named selections on example configuration of 45° convergence half-angle and 15° divergence half-angle.

The mesh was defined by an automatic method, an inflation, and a body sizing. The general mesh was defined by an element size of 0.1", a growth rate of 1.2, and a maximum element size of 0.2".

The inflation was applied to the nozzle wall for a better mesh at the boundary. The inflation was defined by a total thickness of 0.2", a growth rate of 1.2, and 8 layers.

The body sizing was defined by a growth rate of 1.1 and the default element size of 0.1".

The total number of elements in the mesh changes due to the different volumes of each configuration of convergence and divergence half-angles. An example mesh of the nozzle with a  $45^\circ$  convergence half-angle and a  $15^\circ$  divergence half-angle results in a total of 448743 elements (Fig.7) and all meshes were between 425000 and 525000 elements.

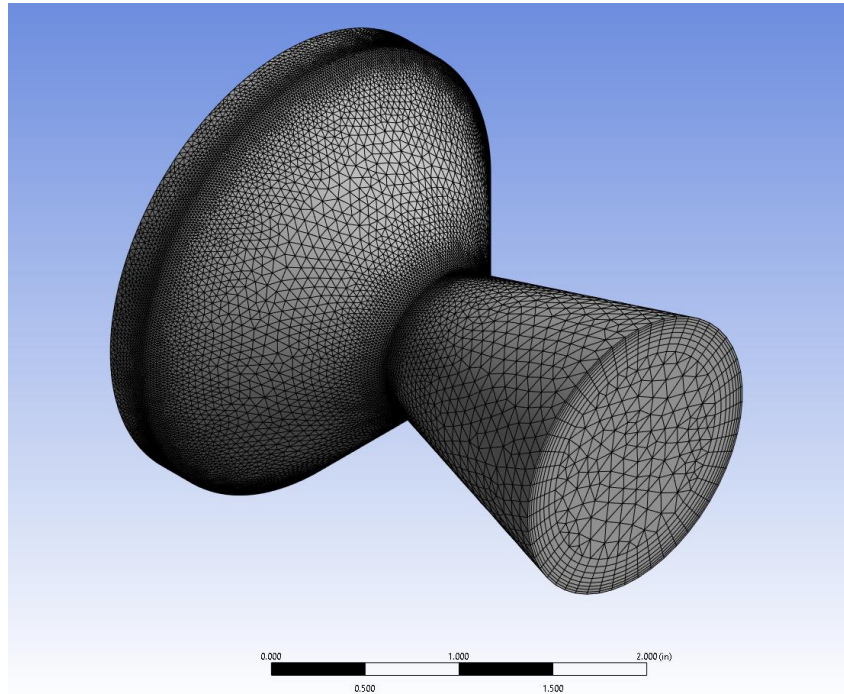


**Figure 7.** Example mesh of nozzle geometry using  $45^\circ$  convergence half-angle and  $15^\circ$  divergence half-angle. The mesh uses an inflation on the nozzle wall and is defined by an element size of 0.1", a growth rate of 1.2, and a total number of 448743 elements.

### *Fluid Properties*

Fluid properties are an important part of this project, as the different properties can significantly affect the flow through the nozzle. The propellant exhaust is a mixture of gaseous and solid particles. However, for the purpose of simplicity, the exhaust will be treated as an ideal gas.

In Ansys Fluent, the required properties to be input for an ideal gas are the molecular weight and the specific heat at constant pressure. The properties of the propellant were found through the use of ProPep3, a software that takes the propellant mixture as an input and outputs various properties of the propellant. The propellant mixture used is "Cherry Limeade" which is an APCP propellant (Fig.8).

The screenshot shows the ProPep3 software interface. On the left, under 'Ingredients', there is a table with columns 'Name', 'Propellant Name', and 'Weight (gr)'. The ingredients listed are AMMONIUM PERCHLORATE (1875.00), CASTOR OIL (7.50), HTPB (R-45M) (272.00), MDI (Desmodur E 744) (48.50), IDP (B. LEE) (107.00), ALUMINUM (PURE CRYSTALLINE) (187.50), and SILICON (PURE CRYSTALLINE) (1.25). Below these, there are several empty rows with a 'Total Wt. (grams)' of 2498.75. On the right, under 'Operating Conditions', there are input fields for 'Temp. of Ingredients (K)' (2700), 'Chamber Pressure (PSI)' (300), and 'Exhaust Pressure (PSI)' (13.20). There is a checkbox for 'Boost Velocity and Nozzle Design' which is unchecked. Below these are buttons for 'Calculate', 'Display Results', and 'Display Nozzle Graphs'. To the right of the 'Calculate' button, the following output values are displayed: Isp\* (191.3714), C\* (4935.778), Density (0.0599274), Molecular Wt. (23.63526), Chamber CP/CV (1.210901), and Chamber Temp. (2808.368).

**Figure 8.** ProPep3 inputs for Cherry Limeade. The formula is 75% ammonium perchlorate, which is the main fuel of the propellant. The chamber pressure is set to 300 psi.

The critical outputs of the propellant from ProPep3 are the molecular weight, the combustion temperature, and the specific heat ratio (Table 2).

**Table 2.** Critical ProPep3 outputs for Cherry Limeade APCP propellant

Fluid Properties		
Molecular Weight (kg/kmol)	Combustion Temperature (K)	Specific Heat Ratio
23.635	2808	1.21

The molecular weight is used as an input for the fluid properties and is also used with the specific heat ratio to calculate the specific heat at constant pressure (Eq.3-5)

$$R = R'/M \quad \text{Eq. 3}$$

$$C_V = C_P - R \quad \text{Eq. 4}$$

$$\gamma = C_P/C_V \quad \text{Eq. 5}$$

Where  $R$  is the specific gas constant,  $R'$  is the universal gas constant,  $M$  is the molecular weight of the fluid,  $C_V$  is the specific heat at constant volume,  $C_P$  is the specific heat at constant pressure, and  $\gamma$  is the specific heat ratio.

Solving these equations provide the following inputs for fluid properties (Table 3).

**Table 3.** Fluid property inputs for Ansys Fluent solver

Fluid Properties		
Molecular Weight (kg/kmol)	Combustion Temperature (K)	Specific Heat $C_P$ (J/(kg K))
23.635	2808	2026.84

The combustion temperature is used as a boundary condition for the inlet, as this is the operating temperature for the propellant to combust.

### *Model*

The nozzle is simulated as an inviscid flow with the energy model on. The fluid model is an ideal gas with the properties of the propellant described previously.

Inlet, outlet, and wall boundaries are applied to the nozzle. The inlet is a pressure-inlet with a total gauge pressure of 300 psi or 2060000 Pa. Additionally, the inlet has a thermal boundary with a total temperature of 2808K which is the combustion temperature of the propellant.

The outlet is a pressure-outlet with a total gauge pressure of 91010.8 Pa. This is the atmospheric pressure at an altitude of about 6700 ft or 2000 m which is the optimized design altitude for the nozzle.

Finally, the wall of the nozzle is an adiabatic, no-slip wall. This is automatically applied by the Ansys Fluent software.

The convergence conditions of the simulation are the continuity, energy, and x-, y-, and z-velocities. Convergence is met when maximum residuals of all conditions are below 1e-06. Should the solution not converge, a maximum of 1000 iterations will be run.

A standard initialization will be used and computed from the inlet.

### *Analysis*

The equation for thrust of the rocket nozzle is dependent on the mass flow rate, the exit velocity, the exit area, and the difference between exit pressure and atmospheric pressure (Eq.6).

$$F = \dot{m}v_e + (P_e - P_o)A_e \quad \text{Eq. 6}$$

Where  $F$  is the thrust,  $\dot{m}$  is the mass flow rate,  $v_e$  is the exit velocity,  $P_e$  is the exit pressure,  $P_o$  is the ambient pressure, and  $A_e$  is the exit velocity.

The exit pressure is defined by the boundary condition to be atmospheric pressure so the term drops out (Eq.7).

$$F = \dot{m}v_e \quad \text{Eq. 7}$$

Mass flow rate for an ideal compressible gas can be calculated using the equation below (Eq.8) [6].

$$\dot{m} = \frac{AP_t}{\sqrt{T_t}} \sqrt{\frac{\gamma}{R}} M \left( 1 + \frac{\gamma-1}{2} M^2 \right)^{-\frac{(\gamma+1)}{2(\gamma-1)}} \quad \text{Eq. 8}$$

In equation 8,  $A$  is area,  $P_t$  is total pressure,  $T_t$  is total temperature, and  $M$  is Mach number. In this case, total pressure and total temperature are the same as the inlet pressure and inlet temperature.

For a given area, the maximum flow rate occurs when Mach number is sonic ( $M=1$ ). This means that the maximum mass flow rate through the nozzle is determined by the throat area. Additionally, conservation of mass means that mass flow rate is constant throughout the nozzle. Since the throat area is constant across all nozzle configurations, this results in the mass flow rate being equal for each configuration of convergence and divergence half-angles. This means that in the simulations, the thrust optimization is only dependent on the exit velocity of the propellant exhaust.

Therefore, the analysis to optimize the rocket nozzle converging and diverging angles consists of determining the configuration with the maximum exit velocity. The exit velocity will be determined by a mass-weighted average of the x-velocity across the outlet boundary outputted using Ansys Fluent's surface integral reports.

The convergence and divergence half-angle optimization will begin by first optimizing the convergence half-angle. The divergence half-angle will be set to  $15^\circ$  and the convergence half-angle will be varied from  $10^\circ$  to  $80^\circ$ . Five different convergence angles of  $10^\circ$ ,  $30^\circ$ ,  $45^\circ$ ,  $60^\circ$ , and  $80^\circ$  will be analyzed and the resulting exit velocities will be plotted. A best fit curve will be plotted over the results to determine the optimal convergence angle.

Once the optimal convergence half-angle has been determined, the convergence half-angle will be set to the optimal angle and the divergence half-angle will be varied from  $10^\circ$  to  $18^\circ$ . Four different divergence half-angles of  $10^\circ$ ,  $12^\circ$ ,  $15^\circ$ , and  $18^\circ$  will be analyzed and the resulting exit velocities will be plotted. A best fit curve will be plotted over the results to determine the optimal divergence half-angle.

A secondary analysis will be done without removing any terms from Equation 6 to cross check the results. The force produced by each nozzle configuration will be compared to determine the optimal nozzle.

## **Results and Discussion**

### *Results*

The x-velocity and Mach number contours for the converging angles of  $10^\circ$ ,  $30^\circ$ ,  $45^\circ$ ,  $60^\circ$ , and  $80^\circ$  are shown in Figures 8-12.

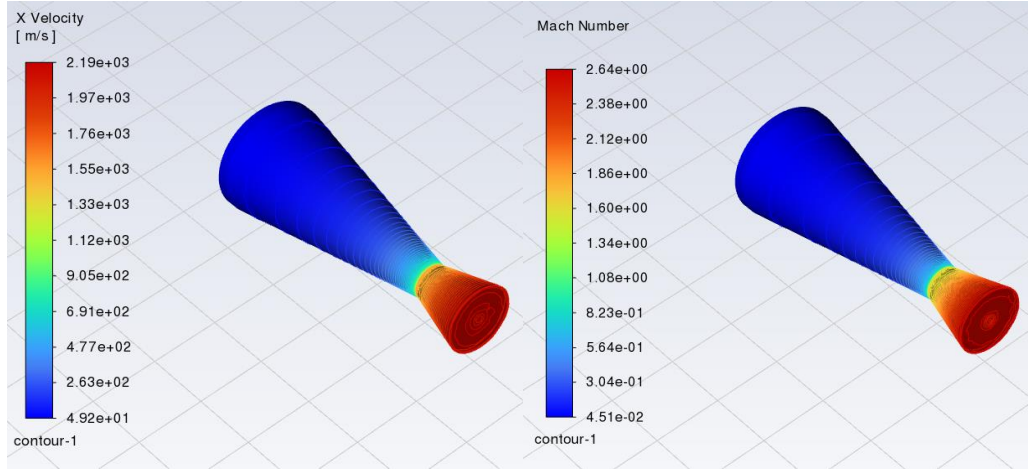


**Figure 8.** Contours of 10° convergence angle and 15° divergence angle nozzle configuration. Left: x-velocity contour. Right: Mach number contour. The Mach number contour shows a Mach number of 1 around the throat area which matches the expected Mach number. Flow in the converging section is subsonic and flow in the diverging section is supersonic.

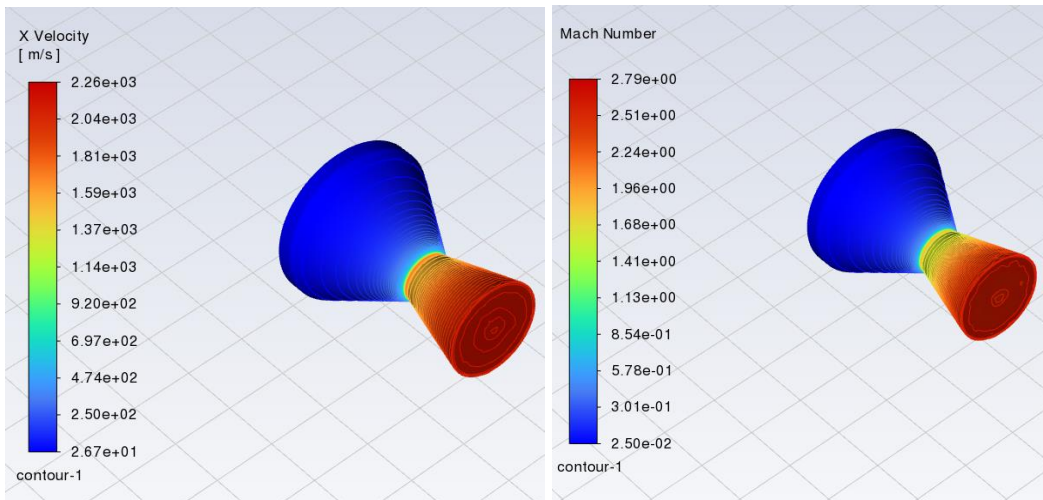


**Figure 9.** Contours of 30° convergence angle and 15° divergence angle nozzle configuration. Left: x-velocity contour. Right: Mach number contour. The Mach number contour shows a Mach number of 1 around the throat area which matches the expected Mach number. Flow in the converging section is subsonic and flow in the diverging section is supersonic.

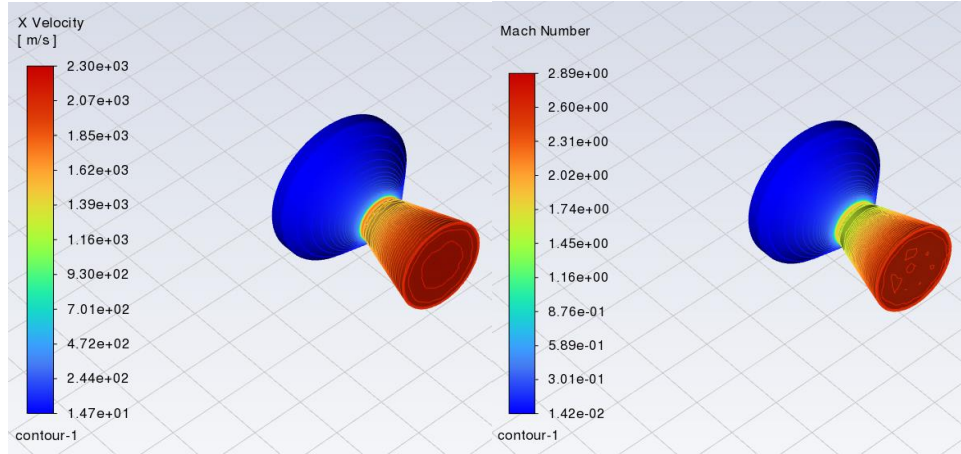


**Figure 10.** Contours of 45° convergence angle and 15° divergence angle nozzle configuration. Left: x-velocity contour. Right: Mach number contour. The Mach number contour shows a Mach number of 1 around the throat area which matches the expected Mach number. Flow in the converging section is subsonic and flow in the diverging section is supersonic.

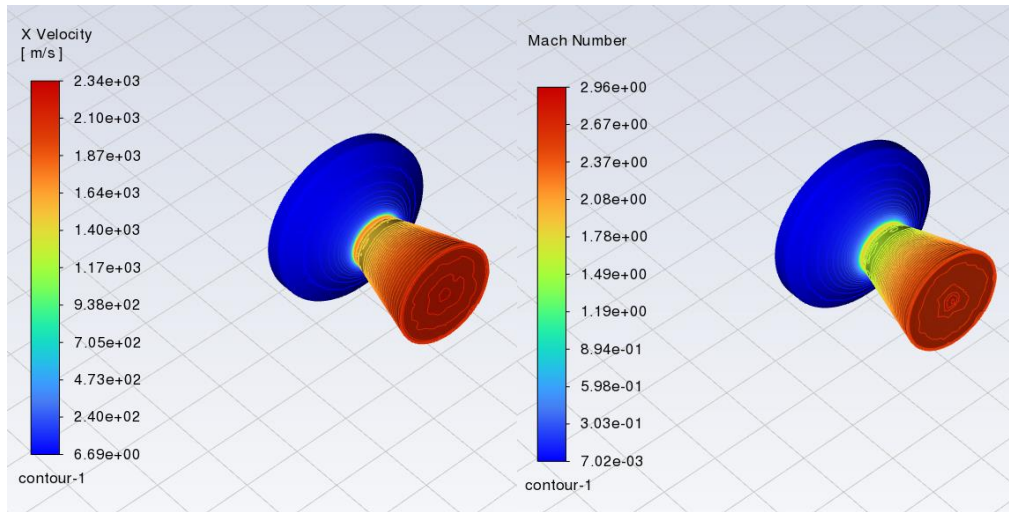


**Figure 11.** Contours of 60° convergence angle and 15° divergence angle nozzle configuration. Left: x-velocity contour. Right: Mach number contour. The Mach number contour shows a Mach number of 1 around the throat area which matches the expected Mach number. Flow in the converging section is subsonic and flow in the diverging section is supersonic.

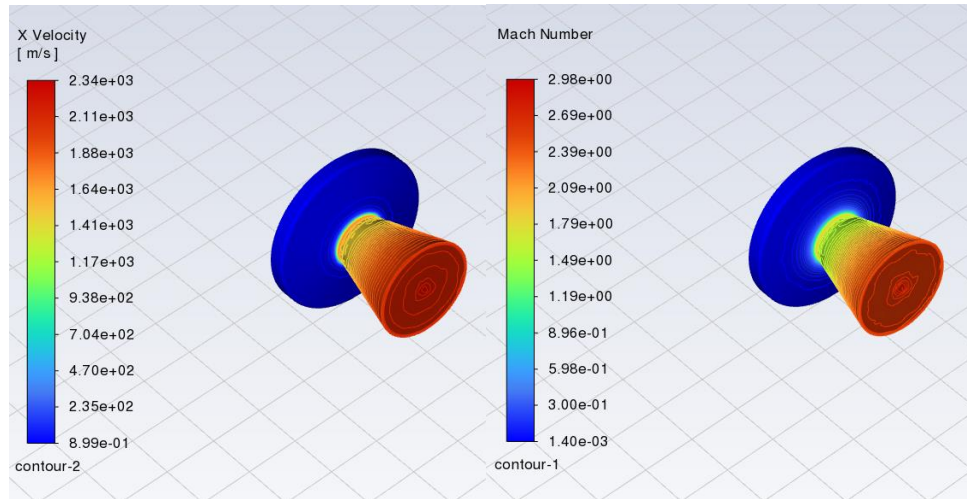


**Figure 12.** Contours of 80° convergence angle and 15° divergence angle nozzle configuration. Left: x-velocity contour. Right: Mach number contour. The Mach number contour shows a Mach number of 1 around the throat area which matches the expected Mach number. Flow in the converging section is subsonic and flow in the diverging section is supersonic.

The angle that results in the maximum exit x-velocity can be seen to be an angle of about 35° (Fig.13) and a simulation at 35° confirms this.

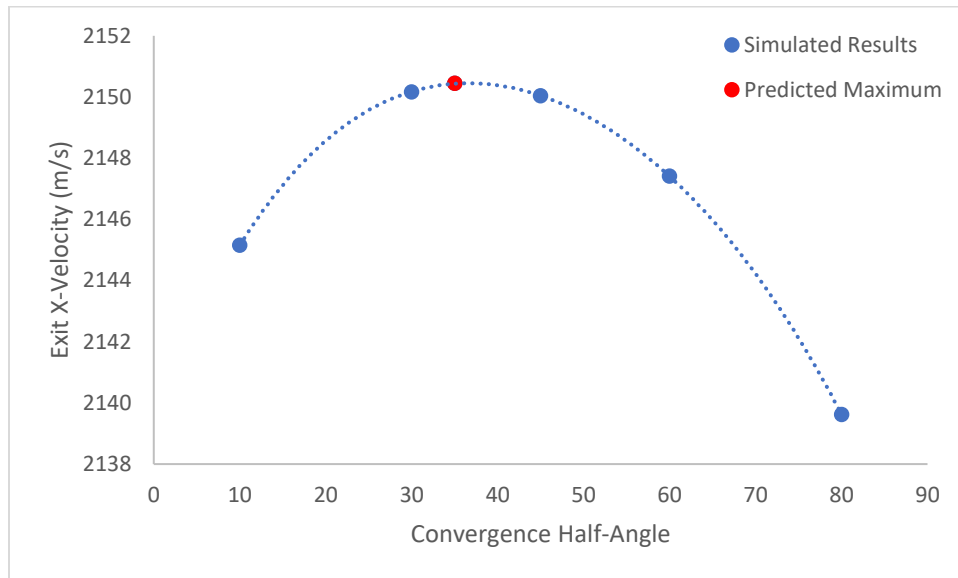


**Figure 13.** Plot of the exit x-velocity (m/s) vs the convergence half-angle in degrees. The maximum predicted by the curve is also plotted. The divergence half-angle was set to 15°. The curve suggests that the convergence half-angle of about 35° provides the highest exit x-velocity.

The results of each pair of angles are shown in Table 4.

**Table 4.** Simulation results for divergence half-angle of 15° and varying convergence half-angles

Convergence Half-Angle	Divergence Half-Angle	Exit X-Velocity (m/s)	Exit Mach Number	Exit Pressure (Pa)	Mass Flow Rate (kg/s)	Thrust (N)
10°	15°	2145.15	2.60	96957	0.476	1029
30°	15°	2150.17	2.61	94401	0.466	1007
35°	15°	2150.45	2.61	93887	0.463	1004
45°	15°	2150.04	2.61	93887	0.463	1000
60°	15°	2147.41	2.60	94405	0.464	1002
80°	15°	2139.62	2.59	97008	0.473	1020

The x-velocity and Mach number contours for the converging angle of 35° at divergence angles of 10°, 12°, 15°, and 18° are shown in Figures 14-17.

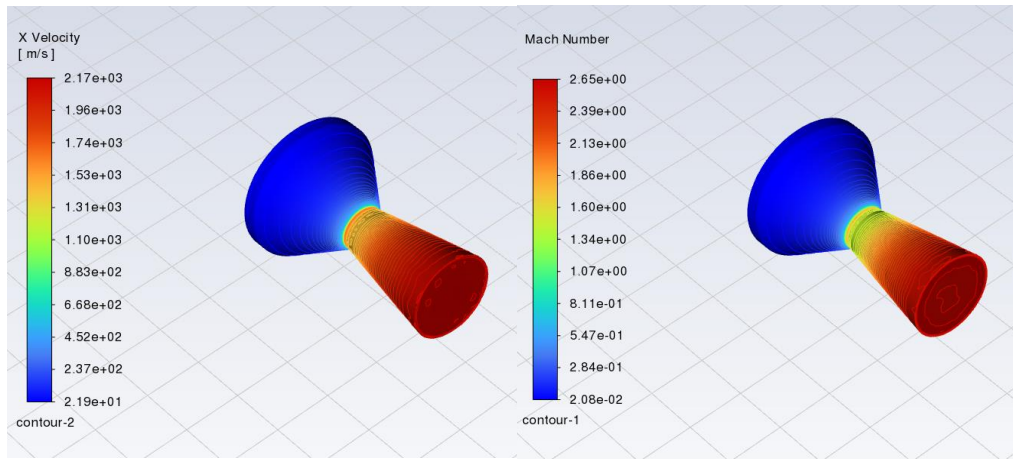


**Figure 14.** Contours of 35° convergence angle and 10° divergence angle nozzle configuration. Left: x-velocity contour. Right: Mach number contour. The Mach number contour shows a Mach number of 1 around the throat area which matches the expected Mach number. Flow in the converging section is subsonic and flow in the diverging section is supersonic.

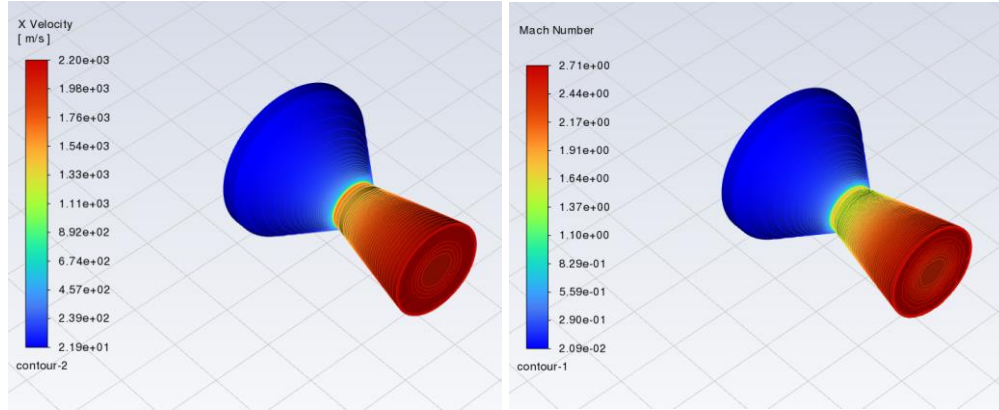


**Figure 15.** Contours of 35° convergence angle and 12° divergence angle nozzle configuration. Left: x-velocity contour. Right: Mach number contour. The Mach number contour shows a Mach number of 1 around the throat area which matches the expected Mach number. Flow in the converging section is subsonic and flow in the diverging section is supersonic.

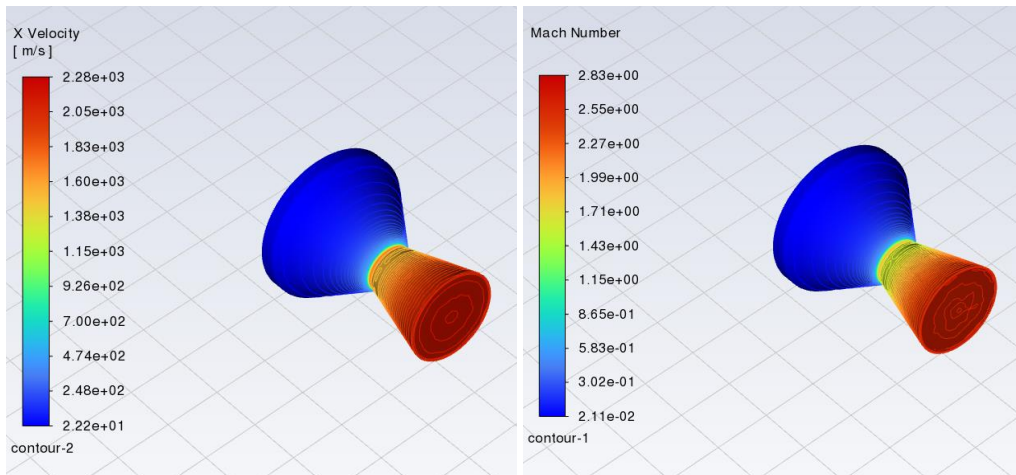


**Figure 16.** Contours of 35° convergence angle and 15° divergence angle nozzle configuration. Left: x-velocity contour. Right: Mach number contour. The Mach number contour shows a Mach number of 1 around the throat area which matches the expected Mach number. Flow in the converging section is subsonic and flow in the diverging section is supersonic.

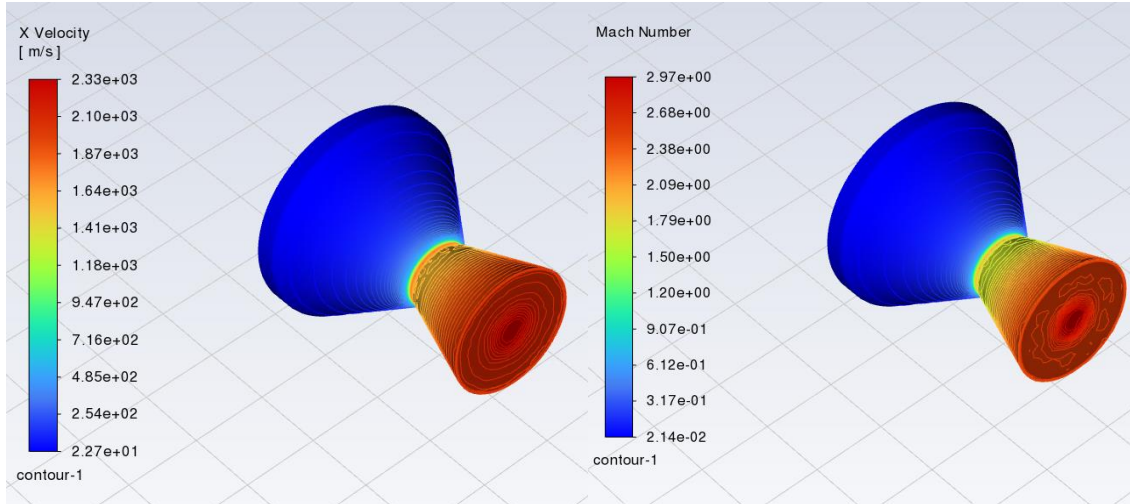


**Figure 17.** Contours of 35° convergence angle and 18° divergence angle nozzle configuration. Left: x-velocity contour. Right: Mach number contour. The Mach number contour shows a Mach number of 1 around the throat area which matches the expected Mach number. Flow in the converging section is subsonic and flow in the diverging section is supersonic.

The angle that results in the maximum exit x-velocity can be seen to be an angle of about 12° (Fig. 18).

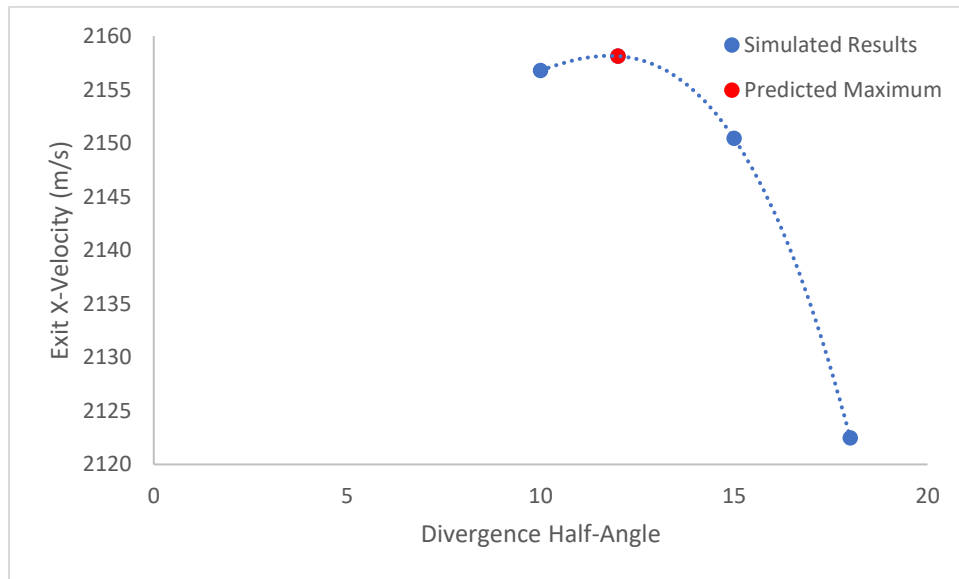


**Figure 18.** Plot of the exit x-velocity (m/s) vs the divergence half-angle in degrees. The maximum predicted by the curve is also plotted. The convergence half-angle was set to determined optimal half-angle of 35°. The curve suggests that the divergence half-angle of about 12° provides the highest exit x-velocity.

The results for each pair of angles are shown in Table 5.

**Table 5.** Simulation results for convergence half-angle of 35° and varying divergence half-angles

Convergence Half-Angle	Divergence Half-Angle	Exit X-Velocity (m/s)	Exit Mach Number	Exit Pressure (Pa)	Mass Flow Rate (kg/s)	Thrust (N)
35°	10°	2156.78	2.62	92898	0.467	998
35°	12°	2158.13	2.61	93390	0.463	1002
35°	15°	2150.45	2.61	93887	0.463	1004
35°	18°	2122.48	2.59	96515	0.467	999

The results show that the optimal convergence and divergence angles for the AstroJays nozzle are 35° convergence angle and 12° divergence angle. The resulting thrust of the optimized nozzles under the problem conditions is 1002N.

### *Discussion*

The nozzle simulations seem to produce valid results, as the Mach number is about 1 at the throat for all configurations of angles. This is the expected throat Mach number for a properly designed rocket nozzle.

Typically, the ideal convergence and divergence angles are a convergence angle of 30-45° and a divergence angle of 15° [8]. The results of the convergence angle fall inside the literature range, but the divergence angle is different. This could be due to some errors in the computation results, as the final inlet and outlet pressures are different than the boundary conditions provided. However, the simulation results are close to the literature as the second-best angle simulated for the divergence angle was 15°.

Another potential source of the difference is the use of a different fluid for the material. The literature uses the ideal gas of air while the simulations presented use the material properties of the propellant instead. The effect of different material properties on the ideal angles can be further explored in a different study, but is beyond the scope of this study.

A third potential source of error is that the optimal angle was based on maximizing the x-velocity of the nozzle. The larger divergence angle of 15° could have resulted in more velocity in the radial direction rather than the x-direction which produces useful thrust while the lower divergence angle of 12° could have less radial velocity.

An interesting result is that the simulation outputs different exit pressures and mass flow rates for each nozzle configuration despite the initial conditions being the same. This contradicts that the mass flow rate should be the same for each nozzle because the throat diameters are equal. This could be due to the inclusion of the 0.1" fillets. As the angles are changed, the fillets may affect the geometry enough that the throat diameter is changed. The different exit pressures and mass flow rates significantly affect the thrust calculated using Equation 6.

When considering the calculated thrusts to determine the optimal convergence half-angle, the simulations suggest that the 80° angle and 10° angle are the best angles while the angles closer to 45° are the worst. This is contradictory to both the literature and the velocity results. The main

cause of this is the discrepancies in the mass flow rate between each configuration. While the mass flow rate should be equal across all configurations based on theory, changing the angle has affected the mass flow rate. One reason for this could be that each solver iteration changes the inlet and outlet pressures from the inputted boundary condition values. By changing these pressures, the mass flow rate is changed as can be seen from Equation 8.

The same issue occurs when varying the divergence half-angle, although in a less significant way. The best two angles are still the  $12^\circ$  and  $15^\circ$  half-angles although the two angles swapped orders.

The simulation could be improved by increasing the quality of the mesh. While the mesh is already of a fine quality, no mesh convergence analysis was done for this study. Determining mesh convergence could lead to more consistent results across the different nozzle configurations.

A next step that could be taken is to study the transient simulation of the nozzle with an additional rectangular domain attached to the outlet (Fig.19). This can provide useful information on the ambient pressures where the nozzle is over and under expanded to determine the optimal altitude for the nozzle.

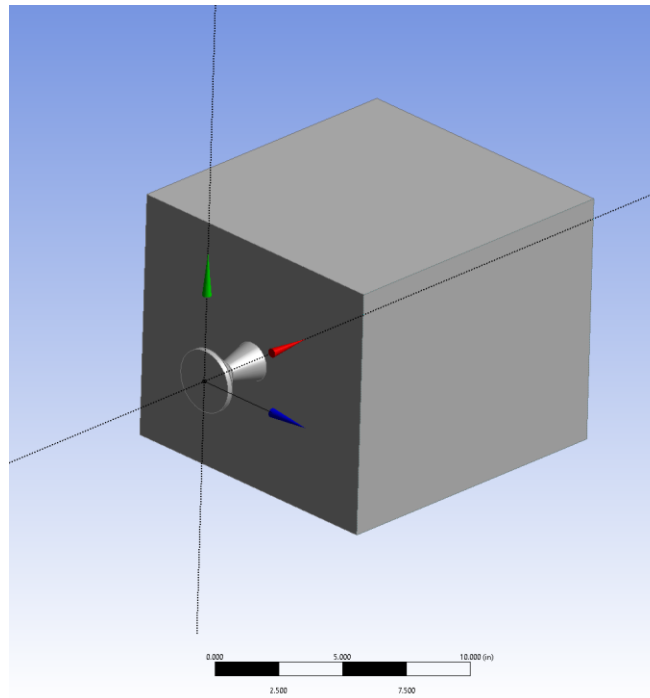


**Figure 19.** Potential geometry for studying transient response of the rocket nozzle. This is a possible next step in the project to further study the nozzle flow.

One fault of this simulation is that it does not consider the effects that the converging and diverging angles have on the mass of the nozzle. Because the inlet, throat, and outlet diameters are constant across the different configurations, smaller angles result in longer converging and diverging sections which means added weight to the nozzle. The current optimization is based

solely on the thrust produced by the nozzle, but the inclusion of weight in the analysis could change the results found here.

## References

- [1] Shenoy, A. D., & Hiremath, S. (2021). Study on Effect of Converging Diverging Angle on the Performance Characteristics of a Rocket Nozzle. *International Research Journal of Engineering and Technology (IRJET)*, 8(6), 2019–2022.  
<https://www.irjet.net/archives/V8/i6/IRJET-V8I6359.pdf>
- [2] NASA. (n.d.). *Nozzles*. NASA. <https://www.grc.nasa.gov/WWW/k-12/airplane/nozzle.html>
- [3] Stephenson, Jackson (2018) "Design of Nozzle for High-Powered Solid Rocket Propellant," *Undergraduate Journal of Mathematical Modeling: One + Two*: Vol. 9: Iss. 1, Article 2.  
DOI: <https://doi.org/10.5038/2326-3652.9.1.4895>
- [4] *Rocket nozzle shapes*. Aerospaceweb.org | Aerospike Engine - Rocket Nozzle Shapes. (n.d.).  
<https://aerospaceweb.org/design/aerospike/shapes.shtml>
- [5] R. Baidya, A. Pesyridis, and M. Cooper, “Ramjet Nozzle Analysis for Transport Aircraft Configuration for Sustained Hypersonic Flight“, *Appl. Sci.* 2018, 8(4), 574.  
DOI: <https://doi.org/10.3390/app8040574>.
- [6] NASA. (n.d.-a). *Mass flow choking*. NASA. <https://www.grc.nasa.gov/WWW/K-12/airplane/mflchk.html>
- [7] Nakka, R. (n.d.). Richard Nakka’s Experimental Rocketry Site. <http://www.nakka-rocketry.net/>
- [8] Sapkota, Jeevan & Xu, Yi & Sun, Hai. (2019). Numerical Study on Response Characteristics of Solid Rocket Pintle Motor. *Journal of Aerospace Technology and Management*. 11.  
DOI: <https://doi.org/10.5028/jatm.v11.1050>